JOURNAL OF GEOPHYSICAL RESEARCH, VOL. 94, NO. D15, PAGES 18,521–18,535, DECEMBER 20, 1989

Cloud Cover Analysis With Arctic AVHRR Data 1. Cloud Detection

J. KEY AND R. G. BARRY

Cooperative Institute for Research in Environmental Sciences and Department of Geography, University of Colorado, Boulder

Automated analyses of satellite radiance data have concentrated heavily on low and middle latitude situations. Some of the design objectives for the International Satellite Cloud Climatology Project (ISCCP) cloud detection procedure such as space and time contrasts are used in a basic algorithm from which a polar cloud detection algorithm is developed. This algorithm is applied to Arctic data for January and July conditions. Both advanced very high resolution radiometer (AVHRR) and scanning multichannel microwave radiometer (SMMR) data are utilized. Synthetic AVHRR and SMMR data for a 7-day analysis period are also generated to provide a data set with known characteristics on which to test and validate algorithms. Modifications to the basic algorithm for polar conditions include the use of SMMR and SMMR-derived data sets for the estimation of surface parameters, elimination of the spatial test for the warmest pixel, the use of AVHRR channels 1 (0.7 μm), 3 (3.7 μm), and 4 (11 μm) in the temporal tests and the final multispectral thresholding, and the use of surface class characteristic values when clear-sky values cannot be obtained. Additionally, the difference between channels 3 and 4 is included in the temporal test for the detection of optically thin cloud. Greatest improvement in computed cloud fraction is realized over snow and ice surfaces; over open water or snow-free land, all versions perform similarly. Since the inclusion of SMMR for surface analysis and additional spectral channels increases the computational burden, its use may be justified only over snow and ice-covered regions.

1. INTRODUCTION

The important role that polar processes play in the dynamics of global climate is widely recognized [*Polar Research Board*, 1984]. The variation of cloud amounts over polar ice sheets, sea ice, and ocean surfaces can have important effects on planetary albedo gradients and on surface energy exchanges [*Barry et al.*, 1984; *Shine and Crane*, 1984]. Cloud cover exerts a major influence over the amount of solar and longwave radiation reaching the surface, and is linked to the sea ice through a series of radiative, dynamical, thermodynamic and hydrological feedback processes [*Saltzman and Moritz*, 1980]. Extent and thickness of sea ice influences oceanic heat loss and surface albedo which thereby influences global climate via the ice-albedo feedback [*Budyko*, 1969]. In turn, sea ice extent is controlled at least in part by radiative input from above.

Previous research in global cloud analysis has made clear the need for cloud retrieval procedures specific to particular climate regimes [*e.g., Rossow*, 1989; *Rossow et al.*, 1989*a*, *b*]. Current procedures for automated analyses of satellite radiance data have been developed for low and middle latitudes but their application to polar regions has been largely unexplored. Those that have been applied to polar data often fail in the polar regions for a number of reasons including: snow-covered surfaces are often as reflective as the clouds, the thermal structure of the troposphere is characterized by frequent isothermal and inversion layers; the polar darkness during winter makes data collected in the visible portion of the spectrum largely unusable; satellite radiometers operate near one limit of their performance range due to extremely low surface temperatures and solar illuminations; there is a maximum concentration of aerosols in spring when the solar zenith angle is large increasing scattering of visible energy; and rapid small-scale variations, which in lower latitudes signify changes in cloud cover, occur on the surface as a result of changes in snow and ice distributions so that clear scenes are much more variable here than in lower latitude regions.

Generally not all of these difficulties are encountered at any one location. However, because they can result in rapid small-scale variation from one location and time to another, a complex analysis method that can recognize and cope with these situations is necessary [*World Meteorological Organization (WMO)*, 1987]. The purpose of this paper is to present a cloud detection algorithm specifically for Arctic AVHRR data, based on ideas of the International Satellite Cloud Climatology Project (ISCCP) algorithm [*Rossow et al.*, 1985]. The procedure used as a starting point in this paper is a test version that shares some of the important features of the final ISCCP version [*Rossow et al.*, 1988], such as space and time contrast, but also has some significant differences. Both summer and winter data are examined, although emphasis is placed on the summer analyses. Additionally, emphasis is placed on Arctic analyses, although many of the ideas also apply to Antarctic data.

2. BACKGROUND

Techniques for cloud detection from satellite data have been developed for use with visible, near-infrared, and thermal data, and have been based on threshold methods, radiative transfer models, and

Paper number 89JD01377.
0148-0227/89/89JD-01377$05.00

statistical classification schemes. A brief summary of some of the important methods is given here; an historical listing of cloud algorithms is given by *Rossow et al.* [1989*b*].

Cloud analysis methods which have included models of the physical properties involved in cloud formation have been developed by *Shenk and Curran* [1973], *Shenk et al.* [1976], *Susskind et al.* [1987], and *d'Entremont* [1986]. Bispectral threshold methods have been developed by *Inoue* [1987*a*], *Minnis and Harrison* [1984], *Minnis et al.* [1987], and applied to polar data by *Inoue* [1987*b*]. The effect of inaccurate snow cover information on retrieved cloud amount in the United States Air Force nephanalysis system was examined by *McGuffie and Robinson* [1988].

To aid in the determination of clear-sky radiances, the spatial aspects of cloud decks and ocean surfaces were examined by *Coakley and Bretherton* [1982], who developed the spatial coherence method. This was extended to two-layer systems by *Coakley* [1983] and *Coakley and Baldwin* [1984]. The spatial coherence method has also been applied by *Crane and Anderson* [1984] and *Ebert* [1989] for the analysis of polar clouds from AVHRR data. A variety of histogram and coherence threshold methods were tested by *Saunders* [1986], and *Saunders and Kriebel* [1987]. *Raschke* [1987] developed decision trees for polar cloud detection with AVHRR data.

Statistical classification procedures, most commonly maximum likelihood and Euclidean distance methods, have been applied to cloud analysis by *Desbois et al.* [1982], *Desbois and Seze* [1984], *Bunting and Fournier* [1980], *Bolle* [1985], *Harris and Barrett* [1978], *Pairman and Kittler* [1986], *Ebert* [1987], *Parikh* [1977], *Garand* [1988], *Welch et al.* [1988], and *Key et al.* [1989*a*, *b*]. A further review of cloud detection procedures is given in *Rossow* [1989]. Global scale application of one cloud detection scheme for the determination of surface and cloud parameters is detailed in *Rossow et al.* [1989*a*, *b*].

The International Satellite Cloud Climatology Project (ISCCP) to map clouds with satellite data began in July 1983. Its goal is to provide a uniform global climatology of satellite-measured radiances and from these to derive an experimental climatology of cloud radiative properties. As a basis for developing the ISCCP algorithm, *Rossow et al.* [1985] compared six cloud algorithms. However, the algorithms were not compared in the polar regions, and a separate study was organized to focus specifically on polar cloudiness [*WMO*, 1987]. The current ISCCP algorithm is composed of a series of steps, each of which is designed to detect some of the clouds present in the scene. The general idea in cloud detection is to first isolate the less variable clear scene radiances in the data and then identify the clouds by their alteration of these radiances (compare to *Rossow et al.* [1989*a*]). Spatial and temporal variation are used in the detection of clear pixels; clear-sky composite maps (over 5-day periods) are then constructed. Finally, each pixel is compared to the clear-sky radiances to determine if cloud is present. It has been recognized that reliable detection of cloudiness in the polar regions with the current ISCCP algorithm is particularly difficult, and it has been recommended that the study of clouds over polar regions be continued [*WMO*, 1988].

3. DATA

Satellite data for the polar regions are collected by the TIROS-N (NOAA 6 et seq.), Nimbus, and Defense Meteorological Satellite Program (DMSP) satellites. Visible and thermal data from the NOAA 7 satellite are the primary data source for this study. Passive microwave data from the Nimbus 7 platform are used to aid in surface parameterization. DMSP visible and thermal imagery are used for validation.

The advanced very high resolution radiometer (AVHRR) on board the NOAA 7 polar orbiting satellite is a scanning radiometer that senses in the visible, reflected infrared, and thermal (emitted) infrared portions of the electromagnetic spectrum (1, 0.58-0.68 μm; 2, 0.73-1.0 μm; 3, 3.55-3.93 μm; 4, 10.3-11.3 μm; 5, 11.5-12.5 μm) with a nadir resolution of 1.1 km. Global area coverage (GAC) imagery is a reduced-resolution (3 x 5 km) product created through onboard satellite processing.

First-order calibration of the AVHRR GAC data was performed following the methods described in the NOAA Polar Orbiter Users Guide [*NOAA*, 1984] and *Lauritsen et al.* [1979]. *Brown et al.* [1985] provide additional information on calibration. Channels 1 and 2 were converted to approximate spectral albedo in percent. Channels 3, 4, and 5 were converted to radiance in mW/(m^2 sr cm) then to brightness temperature in Kelvins [*NOAA*, 1984]. AVHRR channel 3, at 3.7 μm, records both reflected and emitted energy. For some analyses, a separation of these two components may be useful [*Raschke*, 1987]. The channel 3 albedo was approximated by subtracting the thermal radiance that would be emitted in this channel from a blackbody radiating at the brightness temperature measured in channel 4. Emissivities in both channels are assumed equal, since no a priori information exists about the cloud and surface types contained in the data.

The typically low water vapor content in the polar atmosphere and the low physical temperatures reduce most atmospheric effects to a point where they may be neglected for the analyses performed here. Approximate corrections for solar zenith angle in channels 1 and 2 were accomplished through a division of the albedo by the cosine of the zenith angle. Bidirectional reflectance and emittance may also affect the spectral characteristics of surfaces and clouds but have been studied extensively only for snow [e.g., *Dozier and Warren*, 1982; *Robock and Kaiser*, 1985; *Steffen*, 1987]. In the visible channels, bidirectional reflectance may be useful in distinguishing haze from cirrus [*Gerstl and Simmer*, 1985]. Again, correcting for this effect would require a priori knowledge of surface and cloud types in the data, therefore, no corrections for these effects are made.

The Nimbus 7 scanning multichannel microwave radiometer (SMMR) is a conically scanning

radiometer that senses emitted microwave radiation both vertically and horizontally polarized in five channels: 6.6, 10.7, 18.0, 21.0, and 37.0 GHz. Instantaneous field of view of the sensor varies with channel, ranging from 148 x 95 km for the 6.6-GHz channel to 55 x 41 km and 27 x 18 km for the 18- and 37-GHz channels, respectively. The 18- and 37-GHz channels are employed here. No distinction is made between day, night, and twilight orbits; data from overlapping orbits are averaged to yield a daily value. Sea ice concentration was calculated from SMMR data using the operational NASA Team algorithm [*Cavalieri et al.*, 1984]. The 18- and 37-GHz polarization and gradient ratios are used to calculate ice type (i.e., first-year or multiyear) and concentration. A simple gradient ratio threshold is included to reduce the effects of ocean surface spray and foam on ice parameterization [*Gloersen and Cavalieri*, 1986].

AVHRR and SMMR data are merged in digital form to a polar stereographic grid. This projection yields equal-area pixels true at 70° latitude with a 5-km pixel size, a slight degradation of the GAC resolution. The SMMR data were converted to the five kilometer cells by simple duplication of pixels. Further details are given in *Maslanik et al.* [1989].

Three areas of the Arctic are examined (Figure 1). One area is centered on the Kara and Barents Sea extending north to the pole and south to Norway and the Siberian coast. The second area covers most of the Canadian Archipelago and Greenland, and extends north to the pole. The third area extends from the coast of Norway to Ellesmere Island. A 7-day summer series (July 1-7, 1984) of areas 1 and 2, and a winter series (January 6-12, 1984) of area 3 were examined. These data are part of an ISCCP test data set. While covering only one-third of the Arctic Basin, they include representative samples of all surface types found in the Arctic: snow-covered and snow-free land, sea ice of varying concentrations, open water, and permanent ice cap. In fact, these areas during the July period present particularly difficult conditions for cloud algorithms to work with; sea ice is moving, snow is melting and ponds form, and the extensive coastlines exhibit mixed temperature regimes. In the study areas reflectances were found to vary significantly over one week intervals and north-south temperature gradients were observed. A portion of each study area is shown in Figure 2 where AVHRR channel 1 (visible) data on July 3, 1984 are shown for study areas 1 and 2; study area 3 on January 8, 1984 is displayed in AVHRR channel 4 (thermal).

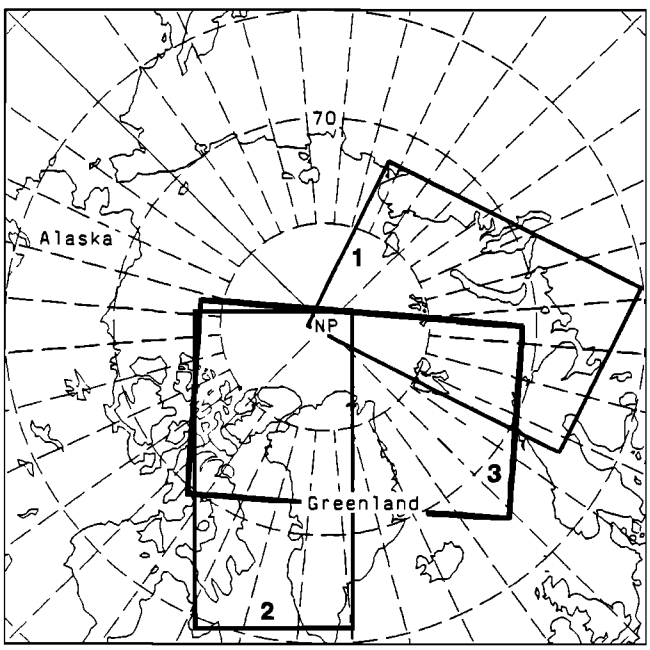

Fig. 1. The three study areas within the Arctic, one centered on the Kara and Barents Sea and the other two covering much of the Canadian Archipelago and northern Greenland.

These conditions are usual for summer in the Arctic, as are the pressure patterns which occurred. Surface pressure maps constructed from Arctic Ocean buoy data taken from *Colony and Munoz* [1986] provide an overall synoptic picture of daily weather which resembles the mean monthly pattern [*Serreze and Barry*, 1988; *Gorshkov*, 1983]. Conditions during the January study period are also similar to the monthly mean pattern. Although correlations have been observed between synoptic pressure systems, cloud amount, and cloud type [*Barry et al.*, 1987], detailed cloud climatologies for the Arctic are not available and it is therefore more difficult to make such a statement concerning cloud cover.

Visible (0.4-1.1 μm) and thermal (10.5-12.5 μm) imagery from the DMSP, a near-polar orbiter with a resolution of 2.7 km for orbital swath format images, was used for manual comparisons of cloud type and amount and surface conditions in cloud-free areas. Other ancillary data include surface temperatures from the European Centre for Medium Range Forecasting (ECMWF), and sea ice albedo from *Scharfen et al.* [1987], which are derived from a combination of DMSP imagery and the NOAA/Navy ice charts.

In order to test the sensitivity of the various cloud algorithms, a control data set with known characteristics was needed. A synthetic data set was developed which consists of seven days of AVHRR data (channels 1, 3, 4), 3 days of SMMR brightness temperature data (every other day; 18- and 37-GHz vertical polarization), SMMR-derived sea ice concentrations, and a land mask. The procedure followed is to first generate the surface and cloud type maps for each day of the 7-day period. Surface types are snow-covered and snow-free land, open water, and sea ice. Cloud layers are classified as low, middle, and high, where levels are defined by AVHRR channel 4 temperatures (T) as follows: low cloud $T > 265$ K, middle cloud $245 \leq T \leq 265$ K, and high cloud $T < 245$ K. The minimum and maximum allowable sizes of surface "objects" (i.e., a single surface type surrounded by other surface types) for the first day, and cloud objects for each day are specified. An object is generated whose dimensions are randomly chosen within the restricted range, and the class of the object is randomly assigned (uniform random number generator).

Regions are then filled with data for each AVHRR and SMMR channel and for sea ice

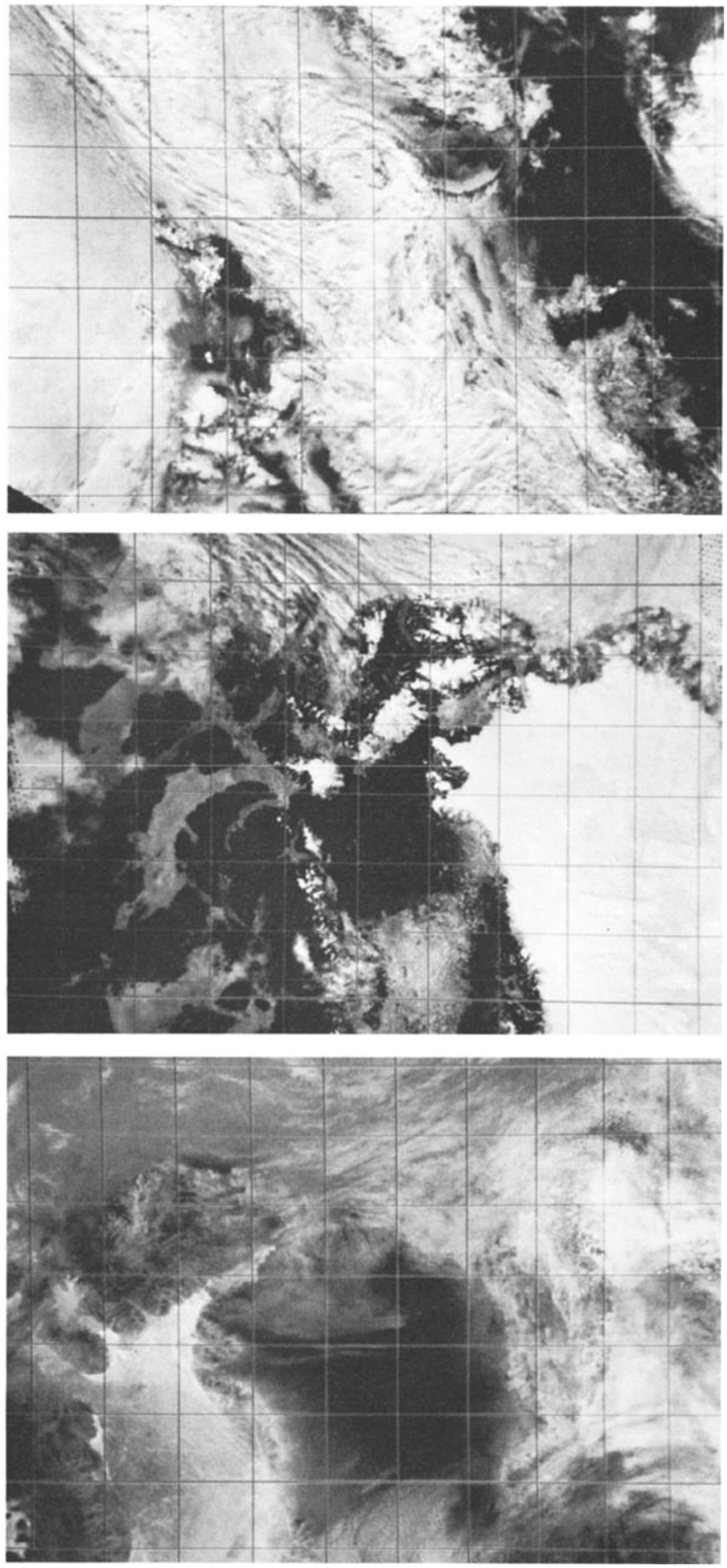

Fig. 2. AVHRR channel 1 (visible) images showing a portion of each summer study area (July 3, 1984; top and middle) and an AVHRR channel 4 (thermal) image of the winter study area (January 8, 1984; bottom). In study area 1 (top), Novaya Zemlya is top center though largely obscured by cloud, Spitsbergen is lower left, and the north pole is just off the lower left of the image. Sea ice occupies the left third of the image. Study area 2 (middle) is centered on Baffin Bay. Sea ice can be seen extending southward to the coast of Greenland. Study area 3 (bottom) is centered on northern Greenland. In this thermal image, lower temperatures are represented by darker grey shades, for example, low surface temperatures over central Greenland and portions of the Canadian Archipelago. See also Figure 1.

concentration using empirically derived statistics. Data were based on class characteristic means and standard deviations computed from training areas. Values for each pixel in each channel were produced using a Gaussian random number generator [*Ebert*, 1989; *Garand*, 1988]. Each artificially generated element of class j is a vector, v_j, of d features:

$$v_j = \mu_j + \Omega A_j$$

where μ_j is the class mean vector of length d, Ω is a vector of random deviations for each feature selected from the multivariate Gaussian distribution of deviations, A_j is the lower triangular matrix decomposed from the d x d class covariance matrix, Σ_j (which is symmetric and positive definite), such that

$$A_j A_j^T = \Sigma_j$$

The values from the Gaussian random number generator have a zero mean and unit variance and are constrained to be in the range of -3 to +3 which include approximately 99% of the data in a normally distributed population.

In the synthetic images, the surface map for the first day and cloud maps for all days are created with this procedure. The surface maps for the third and fifth days, however, are modified versions of the first day. Snow and ice pixels are allowed to melt into land and water, respectively; ice pixels may advance into open water areas and snow may fall on land. The evolution is designed such that approximately 68% of the decisions resulted in an unchanged local area and 32% resulted in either an advance or a retreat.

4. SPECTRAL FEATURES AND CLASSES

Spectral features examined for each pixel are channels 1, 2, and 3 albedos, channels 3, 4, and 5 brightness temperatures, ratios of channels 2 and 1, and the differences between channels 3 and 4 and 4 and 5. The ratio of channel 2 to channel 1 or the difference between channels 2 and 1 enhances vegetation signals as well as snow and sea ice underneath clouds. The reflectance of cirrus clouds is greater than that of snow in the near-IR (channel 2) due to differences in particle effective mean radius, the albedo being higher for smaller grains [*Wiscombe and Warren*, 1980]. Channel 2 wavelengths are less affected by aerosols than are channel 1 responses; snow-free land surfaces have a higher albedo in channel 2 [*Saunders*, 1986]. Because snow- and ice-covered surface albedos decrease with increasing wavelength while cloud albedos decrease only slightly over the same range, channels 1 and 2 of the AVHRR are potentially useful for this discrimination.

Since cirrus clouds have higher transmissivities at channel 3 wavelengths than for channels 4 and 5 [*Hunt*, 1972], corresponding brightness temperatures are higher due to the greater contribution of radiation to the total upwelling radiance by warmer surfaces beneath the cirrus. Therefore channel 3 temperatures will generally be higher than those of the other thermal channels, day or night. This is particularly true for optically thin clouds, and has been modeled by *Olesen and Grassl* [1985]. However, the effect is diminished or even reversed when 3.7 μm emissivities are low, as they are for low water clouds and fog. During the day, the contribution of reflected energy to channel 3 is very low for clear-sky pixels. The albedo of low and middle cloud in this band is much higher, due to a particle size effect. Therefore channel 3 values will be similar to those measured in channel 4 for clear-sky areas. Channel 5 is similar to channel 4, except that channel 5 radiation is more sensitive to water vapor. Therefore in clear, cold atmospheres brightness temperatures measured by the two channels are similar, but channel 5 temperatures may be as much as three percent lower in moist atmospheres [*d'Entremont and Thomason*, 1987]. The brightness temperature difference between channels 4 and 5 is close to zero for stratocumulus but large for cirrus due to differences in emissivities.

Four surface and three cloud classes are analyzed. Surface types are snow-free land, snow-covered land/ice cap, open water, and sea ice. All pixels with ice concentration of at least 15% are classified as sea ice. While cloud detection results may be improved with more than one ice class on a local scale, the use of a single ice class did not produce significantly different results over the entire data set. Cloud classes are defined by brightness temperature in AVHRR channel 4, assumed to represent temperatures at the top of optically thick cloud layers, and encompass the same three temperature ranges as in the synthetic data (low, middle, high).

5. BASIC ALGORITHM

The basic cloud detection algorithm upon which the final polar procedure will be built is based on ideas presented by *Rossow et al.* [1985] as design criteria for the ISCCP algorithm. In particular, space and time contrast tests are two of the major steps used in both early and current ISCCP algorithms, and are employed here. Spatial and temporal variation are used in the detection of clear pixels; clear-sky composite maps are then constucted. Finally, each pixel is compared to these clear-sky radiances to determine if cloud is present. The algorithm assumptions are that cloud scene radiances are more variable in time and space than clear scene radiances and cloudy scenes are associated with larger visible channel and smaller infrared radiances than clear scenes. This algorithm version was tested by ISCCP but is not the final version. The major steps used here are summarized in Figure 3a and are as follows:

5.1. *Spatial and Temporal Variation*

The image is divided into cloudy and "undecided" categories based on cold and warm pixels. If a pixel is much colder (defined later) than the warmest pixel in a small region ((100 km)^2 over land and (300 km)^2 over ocean), it is labeled "cloud." Otherwise, it is labeled "undecided." High and middle level clouds are identified. Only thermal data are used in this step.

Pixels are then compared to the day before and the day after for changes in temperature. If the middle day is much colder than either day, is it is labeled "cloud." If the variation is small, it is

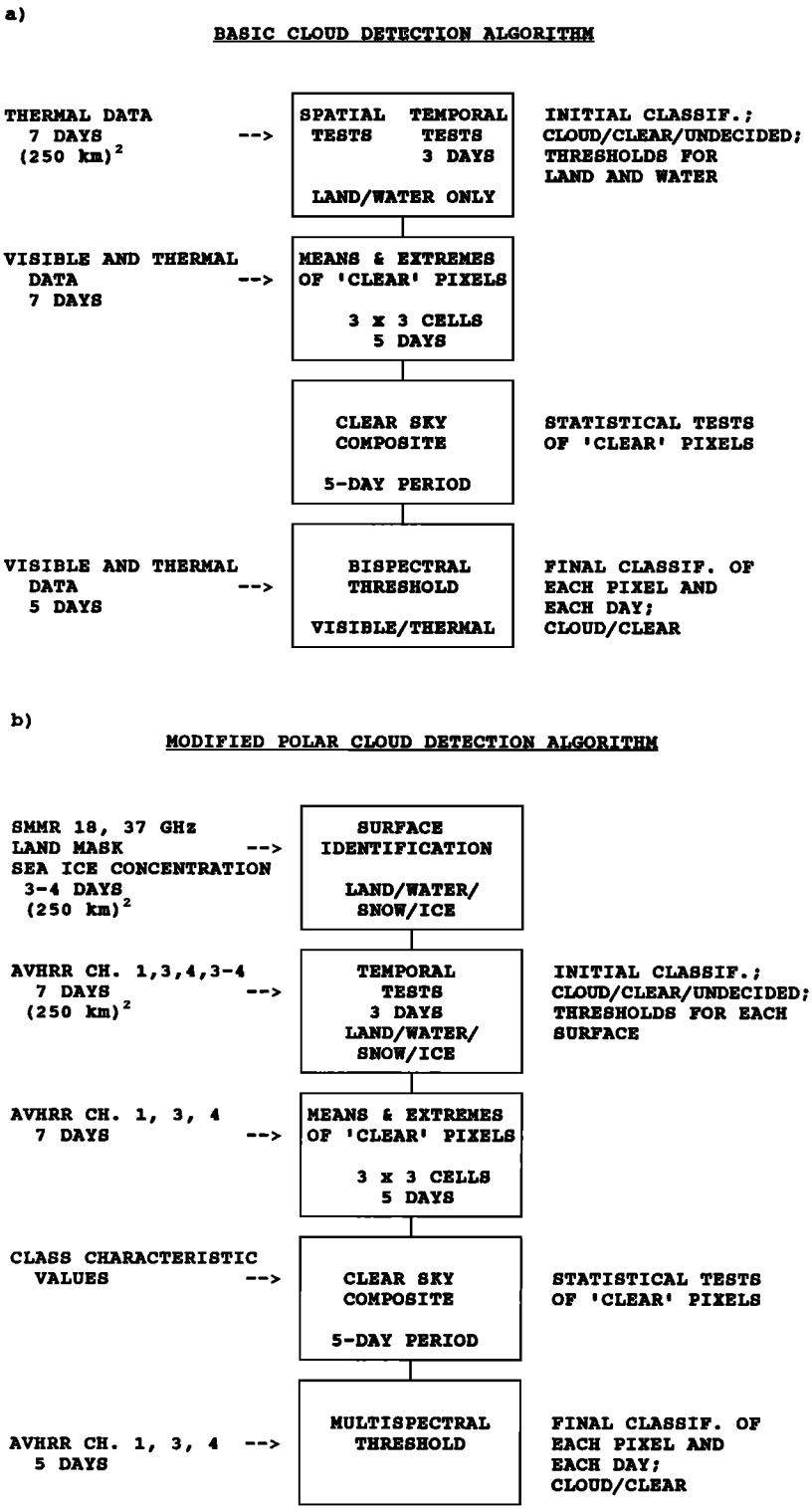

Fig. 3. Flow chart of (a) the basic cloud detection algorithm and (b) the algorithm modified for use in polar regions. Input are shown on the left; additional details are given on the right.

labeled "clear." Those pixels exhibiting intermediate variability are labeled "undecided." Again, only thermal data are used in this step. High and middle clouds are most easily recognized. The class of a pixel based on these two steps is given in Table 1.

5.2. *Compositing*

The mean and extremum radiances for the clear pixels are calculated over 5- and 30-day periods. Statistics are calculated for a 3 x 3 compositing cell centered on the pixel of interest over the time

TABLE 1. Truth Table for the Initial Classification of a Pixel Based on the Results of the Spatial and Temporal Variation Tests

Spatial Variation	Temporal Variation		
	Cloud	Undecided	Clear
Cloud	cloud	cloud	mixed
Undecided	cloud	undecided	clear

period; i.e., 45 pixels are used for the 5-day period. The number and mean of clear pixels only is recorded as well as the maximum temperature and minimum albedo of all pixels, regardless of previous labeling.

The clear-sky radiances for each pixel are then determined. If, as determined by the statistical tests below, the compositing cell associated with a pixel is not variable, the clear-sky value is the mean value over the period, otherwise the extremum (minimum visible and maximum thermal) values are used. The purpose of this and the previous step are to find the most accurate values of clear-sky conditions, therefore the tests are very strict and will probably result in an overestimate of cloud amount.

5.3. *Final Threshold*

The data are compared to the clear-sky values modified by a threshold amount. Those that differ in either the thermal or visible channels by more than the threshold amount are labeled as cloud. This test is less strict than the previous one since the purpose is to detect cloudy conditions rather than clear.

6. MODIFICATIONS

This basic algorithm has been adjusted in order to deal with the problems cited in section 1. Major modifications suggested include the use of snow and ice data sets for the estimation of surface parameters, elimination of the spatial test for the warmest pixel in a subregion, the use of AVHRR channels 1 (0.7 μm), 3 (3.7 μm), and 4 (11 μm) in the temporal tests, statistical tests for compositing, and the final multispectral thresholding, and the use of surface class characteristic values when clear-sky values cannot be obtained. Additionally, the difference between channels 3 and 4 is included in temporal tests for the detection of optically thin low cloud and cirrus. The steps of the modified algorithm are shown in Figure 3b. Some of these modifications require further explanation.

6.1. *Surface Types*

Surface types are determined with a land/ice cap mask, SMMR data, and SMMR-derived sea ice concentration. If the pixel is land, then a SMMR test is applied to determine if the land is snow-free or snow-covered. Snow-covered land exhibits a higher 18-GHz brightness temperature than that of the 37-GHz channel, and the vertical polarization is less variable than the horizontal for land (unless wet). This relationship may not hold over an ice cap, so a mask for permanent ice cap (e.g., Greenland and Novaya Zemlya) is included, and ice cap is then treated as snow. Problems with this method occur in coastal areas where this relationship may be observed even without the presence of snow. Therefore a coastal zone is defined to be approximately 20 km from the edge of the coast both inland and seaward. Finally, if the pixel is not land and if the sea ice concentration is less than 15%, the pixel is labeled water, otherwise it is sea ice.

The basic algorithm assumes a constant surface type over the five-day period. However, snow melt, snowfall, and ice advection cause changes in albedo, emissivity, and temperatures which create difficulties in cloud detection and alter clear-sky composite values. Therefore pixels in which the surface changes during the period are flagged, and receive more than one clear-sky value in the compositing step. Since a 30-day sequence of data was not available, these values are likely to be derived from a small sample of clear pixels, and therefore may not be reliable.

6.2. *Spatial and Temporal Variation Tests*

One of the basic assumptions of the algorithm, that the surface is warmer than the cloud, is often violated in summer polar data and is commonly incorrect during the winter. It is not uncommon in summer for low cloud to be at the same or higher temperature than the underlying snow or ice surface. In winter it is not uncommon for all cloud but cirrus to be warmer than the surface. While use of a spatial test may be possible, it would require knowledge of the temperature profile. This is assumed not to be the case and, for this reason, the spatial variation test for the warmest pixel in a subregion was eliminated entirely.

In the temporal variation test of the initial classification, where pixel temperatures are compared to the day before and after, if a pixel is much colder than either day (by the amount in Table 2, "Cloud") then that pixel is labeled cloud. If the albedo and temperatures are the same as either day (Table 2, "Clear") in channels 1, 3, and 4 then the pixel is labeled clear. Otherwise, it is labeled undecided. Obvious problems occur when warm, low clouds move into or out of a region where the surface temperature is within the "clear" range of the cloud. These cloudy pixels will consequently be labeled

TABLE 2. Temporal Thresholds by Surface Type

	Land	Ocean	Ice	Snow
Cloud if greater				
Channel 4	8.0	3.5	5.0	7.0
Clear if within				
Channel 1	4.4	1.4	8.8	3.8
Channel 3	4.0	3.5	3.5	3.5
Channel 4	2.5	1.1	2.0	2.0

A pixel is compared to the same location on the day before and the day after. Channel 1 values are percent albedo; channels 3 and 4 are Kelvins.

clear in this step, and will ultimately be labeled clear and used in the compositing step to determine clear-sky radiances. Since thermal-only tests fail to label these pixels correctly, channels 1 and 3 data were also used in the temporal variation test. Values in Table 2 were derived experimentally except for channel 4 land and ocean temperatures which are taken from ISCCP specifications.

To reduce the computational burden, a test for a large difference between channels 3 and 4 is done. If the difference is greater than 3.5 K [*Saunders*, 1986; *Olesen and Grassl*, 1985], the pixel is labeled cloud and is not compared to the day before and after. Spatial/temporal tests which included the entire 7-day period were also tested. However, problems with the warmest pixel being low cloud were too frequent to justify their use.

6.3. *Compositing*

To determine clear-sky composite values, distributions of those pixels initially labeled clear are tested for cloud contamination. The idea is that if a large enough sample of clear values for a given location is available, an average of this sample will provide a better clear-sky composite value than the extrema radiances. Conversely, if only a few clear values were obtained in the initial classification, the extrema provide the most reliable estimate upon which to base the final cloud detection. "Populations" against which to test compositing cell statistics are based on class characteristic means and standard deviations for each surface type are computed and updated with each region analyzed. These values are initially set to those determined for the previous 5-day period, or from training area statistics based on manual interpretations if no previous data are available. (Class characteristic values for polar surfaces and clouds in AVHRR data are also given in *Ebert* [1988, 1989].) Those clear-sky composite mean values which pass the statistical tests are incorporated into the new class characteristic values.

The statistical tests are designed to determine the likelihood that the clear pixels in each compositing cell are in fact all clear. This is done by examining the mean, standard deviation and extremum of the distributions of radiances in each cell. The procedure followed here first checks the number of clear pixels in the compositing cell (maximum 45). The cutoff value for too few pixels is a sample size such that the population mean could be predicted from the sample mean to within one population standard deviation (arbitrary) at a specified confidence level; e.g., at a level of confidence of 0.99, this criterion requires that sample statistics and further tests be based on at least seven clear pixels. If the number of clear pixels is less than seven, then the maximum thermal and minimum visible values are used in the clear-sky composite, assuming that the probability of them coming from the appropriate population (t test) is greater than the specified level of significance.

If, on the other hand, the number of clear pixels is sufficient, the probability that the minimum thermal and maximum visible values come from the population is also tested. If the probability of obtaining either a smaller thermal or larger visible value is less than the significance level, cloud contamination is assumed and the opposite extrema are used as the clear-sky composite values. Otherwise, a t test is perfomed on the means of the composite cell and the class characteristic values where the null hypothesis is that the means of the respective populations are equal. If the null hypothesis in both tests is not rejected, then the mean values are used as the clear-sky composite. Otherwise, extrema are used.

The assumption of Gaussian distributions that these tests carry may be violated if data are examined over large spatial and temporal scales. In such cases, an informational class such as land albedo may comprise more than one statistical class. It is therefore important that class characteristic values be computed for relatively small geographic areas and time scales. In this study, radiance means and variances are derived from (250 km)^2 areas over 5-day periods.

If the statistical tests during compositing fail, the clear-sky value for a given location is assigned a value based on its spatial neighbors or class characteristic value. The neighborhood of pixels with the same surface type is searched and the first clear value found of the same surface type is used. The maximum search radius is determined by an autocorrelation function derived for each surface type in this data set (up to a radius of 12 pixels or 60 km). If no value is found within this radius, the clear-sky value assigned is based on the class characteristic values.

6.4. *Final Thresholds*

The final thresholding step utilizes AVHRR channels 1, 3, and 4. Channel 3 is used only if the surface is sea ice or snow/ice cap, and is intended to detect low cloud. Middle and high clouds will normally be detected over any surface with thermal data alone. Thresholds for this step were derived empirically and are given in Table 3. They are relatively large so that the algorithm yields a conservative estimate of cloud fraction, in part adjusting for partially covered pixels. Some methods of cloud cover analysis have attemped to set thresholds which account for this condition [e.g., *Coakley and Bretherton*, 1982; *Arking and Childs*, 1985; *Coakley*, 1987]. However, radiances similar to those for partially covered pixels can also be produced by optically thin clouds, and there is currently no reliable method of distinguishing between these two effects [*Rossow et al.*, 1985].

TABLE 3. Final Thresholds for the Three AVHRR Channels

Channel	Land	Ocean	Ice	Snow
1	6.0	3.5	6.0	4.0
3	6.0	6.0	5.0	5.0
4	8.0	3.0	4.0	4.0

Channel 1 values are percent albedo; channels 3 and 4 are kelvins.

Therefore the degree to which pixel values differ from the clear-sky values in each channel is retained by the algorithm and can be used as an indication of the reliability of computed cloud fraction. This procedure follows the one currently employed in the ISCCP algorithm [*Rossow et al.*, 1988].

For analyses presented here, a pixel is labeled cloud if it varies from the clear-sky value by more than the threshold in any channel. The importance of this disjunction is illustrated in Figure 4 where the differences between cloudy pixel radiances and the radiance of the underlying surface, taken to be the clear-sky composite value, are plotted for each channel. The data are based on summer samples taking imagery containing a variety of surface types and cloud distributions. Zero differences are found along the line in each plot. Of particular interest are the points near this line, representing optically thin clouds over ice or snow in channel 1, and low (possibly inversion) clouds in the channel 4 plot. With both a reflected and thermal component in channel 3, there are many possible combinations of surface and cloud top temperatures and reflectivities which would give rise to similar cloud and surface radiances in the middle plot. Over snow and ice, the most common are: optically thick low and middle cloud with reflectivity and temperature similar to the surface, thick cloud with higher reflectivity but lower brightness temperature, or thin low and middle cloud.

6.5. *Winter Analysis*

Surface temperatures over land in January 1984 were typically 225-235 K, ocean (open and thin ice) in the southern portion of the study area was 260-275 K, sea ice was 231-235 K, and clouds ranged from 215 to 258 K. In the final threshold step, the assumption that clouds are colder than the surface was eliminated and the test was modified so that a difference from the clear-sky composite value in either direction signals a cloudy pixel. Additionally, temperatures within the broadly defined surface classes vary considerably across the image, in particular for Greenland snow/ice cap due to elevation change and open water from the Norwegian Sea north to Svalbard. Class characteristic values are no longer reliable, so statistical tests are based only on the range of the extremum.

7. TESTING AND ALGORITHM COMPARISON

Three algorithm versions are compared. The original algorithm (herein "Basic VT") developed for low latitude summer conditions recognizes only two surface types: land and water. No SMMR or sea ice concentration data are employed. Spatial/temporal tests in the initial classification step are thermal only (AVHRR channel 4), and a visible/thermal bispectral threshold test (channels 1 and 4) is used in the final classification. This version with a thermal-only threshold test was also used to simulate winter applications ("Basic T"). The algorithm with modifications decribed in the previous section is the third version tested ("Modified").

Four regions from the AVHRR imagery and four regions from the synthetic data sets, all

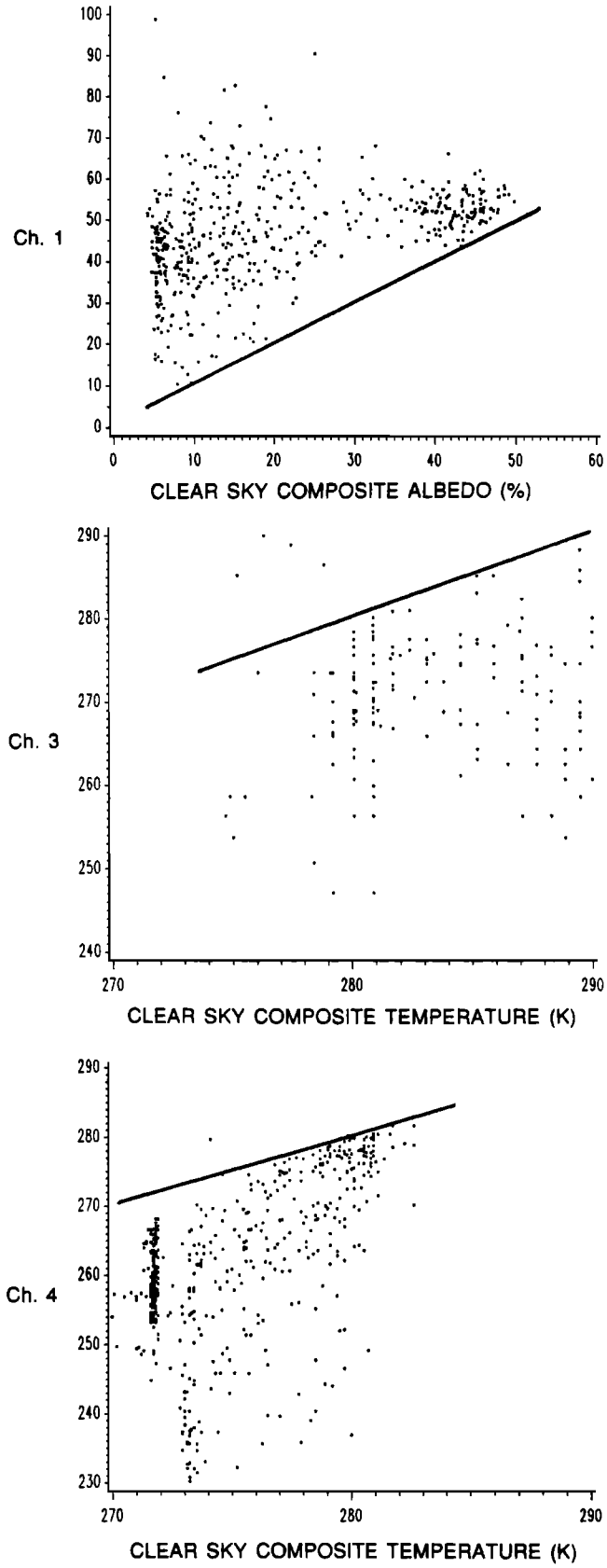

Fig. 4. Five-day clear-sky composite values from the modified algorithm for a sample of pixel locations plotted against AVHRR measured values for the same locations under cloudy conditions. Channels 1 (top), 3 (middle), and 4 (bottom) are shown. The line in each plot represents equal clear-sky composite and measured values.

summertime, are used as test data. Each region is 50 x 50 pixels or (250 km)^2 and differs in surface and cloud types and proportions. The synthetic data set image contains surface areas with 250 to 500 km as the minimum dimension ("objects" are rectangular). Cloud sizes and distributions changed from day to day, with the minimum dimension ranging from 20 to 300 km. Surface proportions changed in both data sets by up to 20%. These changes are due to sea ice movement and melting. The surface/cloud types and proportions are given in Table 4.

TABLE 4. Percentages of Cloud and Surface Types Within the Eight Test Regions

Region	Day	Synthetic Data Low, Middle, High %	AVHRR Data Low, Middle, High %
1	2	4, 28, 39	0, 0, 3
	3	24, 43, 6	72, 18, 0
	4	47, 41, 11	14, 0, 7
	5	6, 0, 81	10, 20, 16
	6	58, 8, 33	52, 10, 33
Surface:		water: 100	ice: 100
2	2	29, 0, 58	12, 12, 75
	3	21, 42, 17	13, 30, 53
	4	30, 12, 16	27, 41, 30
	5	0, 17, 78	18, 43, 38
	6	55, 7, 37	18, 80, 0
Surface:		land: 35, water: 65	water: 100
3	2	0, 33, 0	10, 17, 53
	3	24, 20, 24	17, 33, 10
	4	59, 20, 21	10, 45, 25
	5	0, 0,100	0, 20, 3
	6	20, 25, 16	15, 40, 20
Surface:		water: 24, snow: 76	land: 80, water: 12, ice: 8
4	2	0, 52, 0	5, 10, 82
	3	31, 14, 54	35, 30, 30
	4	12, 0, 28	71, 10, 0
	5	10, 20, 51	28, 25, 7
	6	48, 18, 17	17, 50, 23
Surface:		land: 22, water: 12, ice: 66	water: 45, snow: 27, ice: 22, land: 6

Cloud data are given for the middle five days of the 7-day analysis period. Cloud categories are low, middle, and high. Surface type proportions are given for the first day of the period.

Cloud fractions computed by each algorithm for each region and day are given in Tables 5 and 6. Also given in the table are the number of clear pixels used in the compositing step for each region and version. The actual cloud amount is shown for synthetic data sets, determined by counting the number of pixels in the region assigned to a cloud class. A manual interpretation was done utilizing all AVHRR, SMMR, and SMMR-derived data sets. Due to the subjective nature of this procedure, however, measured cloud fraction should be used only as a "standard" by which to judge algorithm performance and should not be treated as an absolute.

All versions of the algorithm perform best over land and water. Snow and ice remain the problem areas although the modified versions performed best under these conditions. When cloud amounts are high (more than 80%), all versions compute cloud fraction to within approximately 5% of each other.

TABLE 5. "Actual" Cloud Fraction for Synthetic Data and Cloud Fraction Computed by the Three Versions of the Cloud Detection Algorithm

Region	Day	Actual	Algorithm Version: Basic VT	Basic T	Modified
1	2	71	76	76	78
	3	73	80	80	75
	4	99	100	98	100
	5	87	90	90	90
	6	99	100	98	100
Number clear:		...	643	643	125
2	2	87	93	92	94
	3	80	97	97	82
	4	58	83	80	77
	5	95	100	100	95
	6	99	100	98	100
Number clear:		...	219	219	71
3	2	33	82	78	83
	3	68	94	91	94
	4	100	100	94	100
	5	100	100	100	100
	6	61	96	90	97
Number clear:		...	415	415	425
4	2	52	90	76	58
	3	99	99	98	99
	4	40	79	66	54
	5	81	98	95	81
	6	83	96	88	92
Number clear:		...	420	420	32

Values are for each of the middle five days of an analysis period. The number of clear pixels in the compositing step is also shown.

When cloud amounts are low, the modified version is more accurate, although cloud fraction was often too high. In the actual data, this is at least in part due to possible discrepancies in the manual interpretation, as described above. In the synthetic data, this is probably due to the fact that clear-sky areas are filled with values in the range of the mean plus or minus three standard deviations (following a Gaussian probability function), so that extreme values may be beyond threshold cutoffs and will consequently be labeled as cloud. Final thresholds are generally between two and three times the standard deviations used in the generation of synthetic images.

The basic algorithm versions often overestimate cloud amount. This is common over ice where, in the bispectral threshold test, the threshold for water is used. This albedo threshold is too small to account for variation in sea ice albedos, and consequently many clear pixels were mistaken as cloud. A related situation is that the basic version

TABLE 6. Cloud Fraction for Actual (AVHRR) Data as Computed by Manual Interpretation and Three Versions of the ISCCP Algorithm

Region	Day	Manual	Algorithm Version		
			Basic VT	Basic T	Modified
1	2	3	56	2	1
	3	90	99	78	79
	4	21	70	12	10
	5	46	90	65	55
	6	95	99	89	85
Number clear:		...	2404	2404	2264
2	2	99	99	99	100
	3	96	97	81	98
	4	98	94	75	96
	5	99	100	99	100
	6	98	92	73	98
Number clear:		...	159	159	9
3	2	80	83	75	85
	3	60	62	55	61
	4	80	83	73	80
	5	23	31	18	29
	6	75	77	72	77
Number clear:		...	1509	1509	972
4	2	97	100	99	100
	3	97	99	63	98
	4	81	95	46	85
	5	60	76	51	75
	6	90	95	80	92
Number clear:		...	1031	1031	362

TABLE 7. Root Mean Square Error in Cloud Fraction Computed by Each Algorithm Version for the Manually Interpreted Amount in the AVHRR Data and the "Actual" Amount in the Synthetic Data (Tables 5 and 6)

Data Set	Algorithm Version		
	Basic VT	Basic T	Modified
AVHRR	19.8 (11.5)	15.3 (11.3)	6.2 (4.4)
Synthetic	21.0 (14.4)	17.0 (12.0)	16.3 (9.2)

Mean absolute difference is also given (in parentheses).

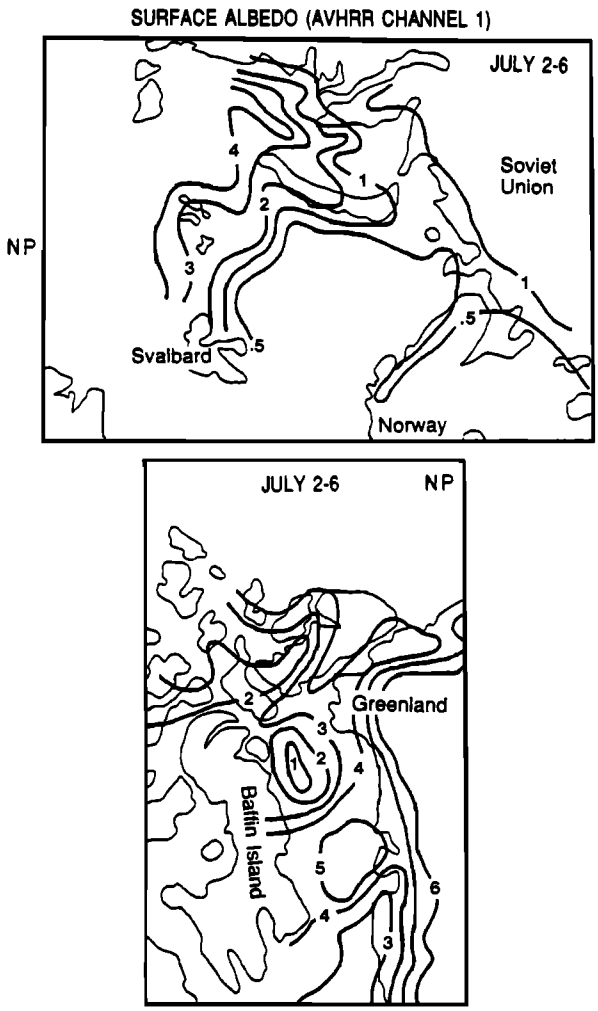

Fig. 5. Surface albedos (AVHRR channel 1) in study areas 1 and 2 for the compositing period July 2-6, 1984, in tenths.

often makes an accurate assessment of cloud fraction, but for the wrong reason. For example, one sea ice region had over 70% of the cloud cover as very thin cloud, possibly haze. Channels 1 and 4 alone did not detect this condition, yet the threshold-determined cloud amount for Basic VT is similar to the amount determined manually. Here again, albedo contributions from the thin cloud are insignificant, so that the algorithm is labeling cloud by the threshold step that it sees in channel 1 as sea ice. The snow and ice data sets used in the modified versions solve these problems by providing appropriate thresholds.

Root mean square and mean absolute difference errors given in Table 7 illustrate that the modified version was most accurate in computing cloud fraction for both data sets. The thermal-only version performed reasonably well with the synthetic data set, at least in part for reasons explained above.

8. APPLICATION

The modified version of the algorithm was next applied to the Arctic study areas. Surface albedos determined over the 5-day compositing period for the two summer study areas, which overlap the winter area, are shown in Figure 5. Values are averages over each quarter of the 250 x 250 km analysis regions. Sea ice albedo from *Scharfen et al.* [1987] is shown in Figure 6 and is in general agreement with Figure 5 for sea ice. A direct comparison is complicated by the difference in resolution, the data in Figure 6 being much coarser and for sea ice only, and because those data are integrated over a broader spectral band. They are therefore expected to be somewhat lower than the albedo measured by AVHRR channel 1, depending on the amount of snow cover present. Composited surface temperatures are shown in Figure 7 for AVHRR channel 4. Since surface emissivities in channel 4

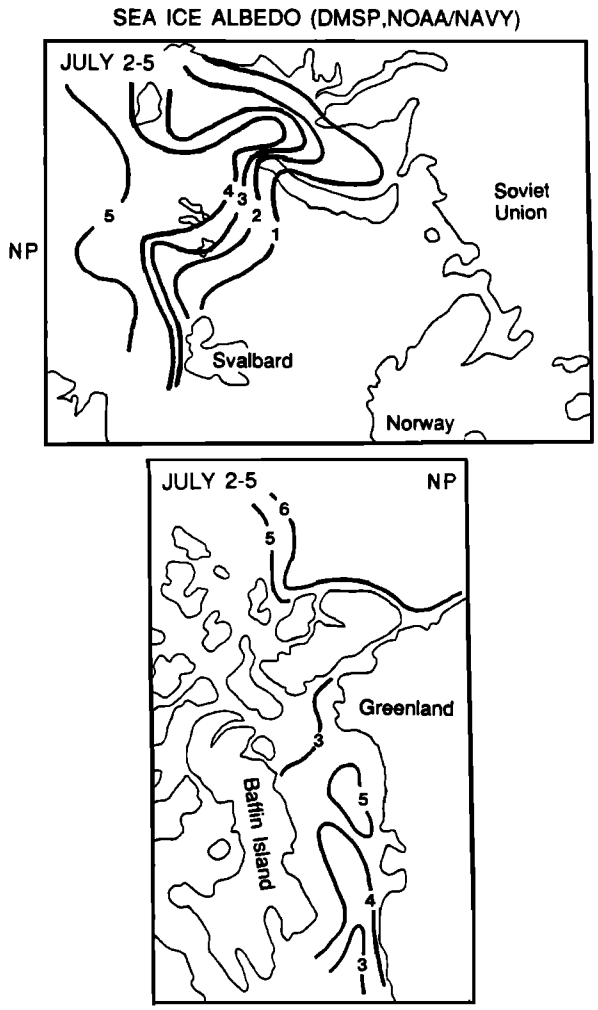

Fig. 6. Sea ice albedos for the period July 3-5, 1984, in tenths. After *Scharfen et al.* [1987].

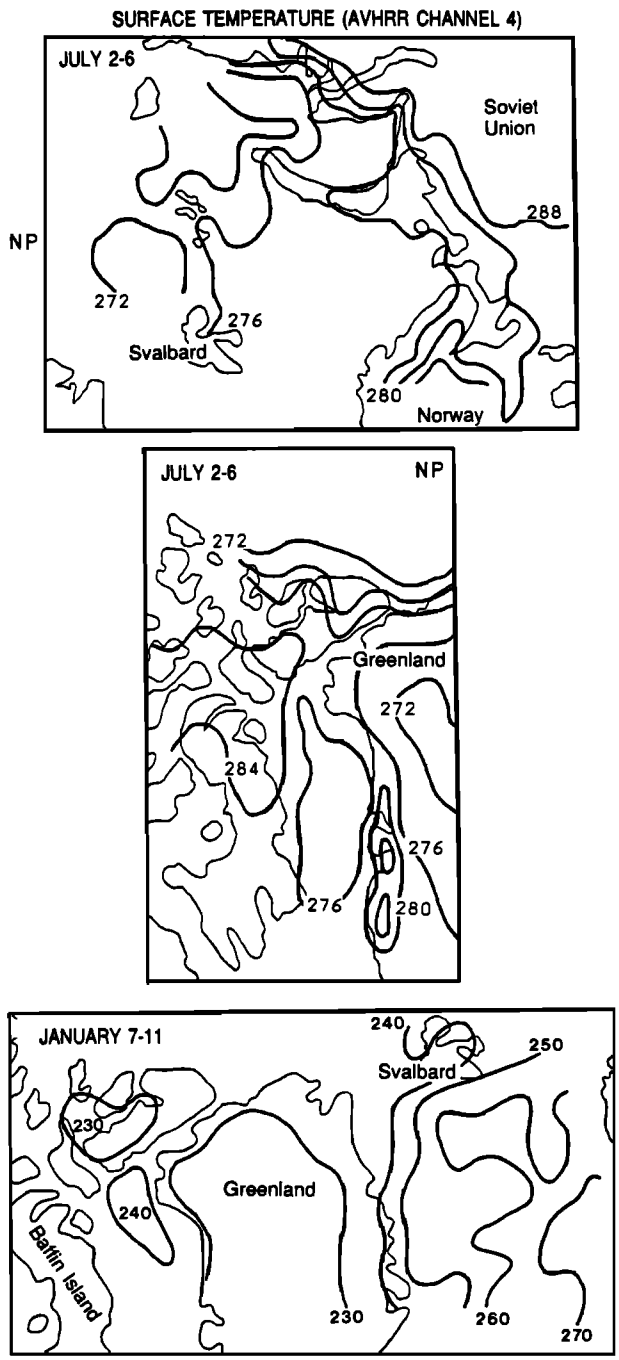

Fig. 7. Surface temperatures (AVHRR channel 4) for the compositing periods, July 2-6, 1984 (top and middle), and January 7-11, 1984 (bottom), degrees Kelvin, for all three study areas.

(11 μm) are near unity, the temperatures presented may be considered as estimates of physical temperatures. These are similar to the ECMWF data presented in Figure 8. Differences are due to the averaging over quarter regions, and to the adjustment of temperatures over Greenland to sea level in the ECMWF data. Winter composite temperatures show greater departures from the meteorological data than the summer values, probably due to invalid lapse rate assumptions in the construction of the ECMWF data.

Cloud fraction for the third day of the analysis period for each study area is shown in Figure 9 and compares favorably with a manual interpretation of the DMSP imagery (not shown) and the images presented in Figure 2. The largest differences occur over sea ice where low cloud cannot be distinguished in the DMSP visible and thermal channels alone. In these cases the DMSP-estimated cloud fraction is too small, as cloud is mistaken as sea ice. Similarities can also be seen between the computed cloud amount and the mean for July given in *Gorshkov* [1983], where the cloud amount increases to 0.9 toward the pole. Near Novaya Zemlya and also across the Canadian Archipelago cloud amounts of 0.7-0.8 in the July mean are typical. For the winter period, no visible data are available, so that accuracy assessment through a comparison with manual interpretations is more difficult. However, an examination of surface temperatures did not appear contaminated, so that cloud fraction computed by the threshold step should be reliable.

9. DISCUSSION

The initial classification step is the most difficult part of the algorithm to refine due to its sensitivity

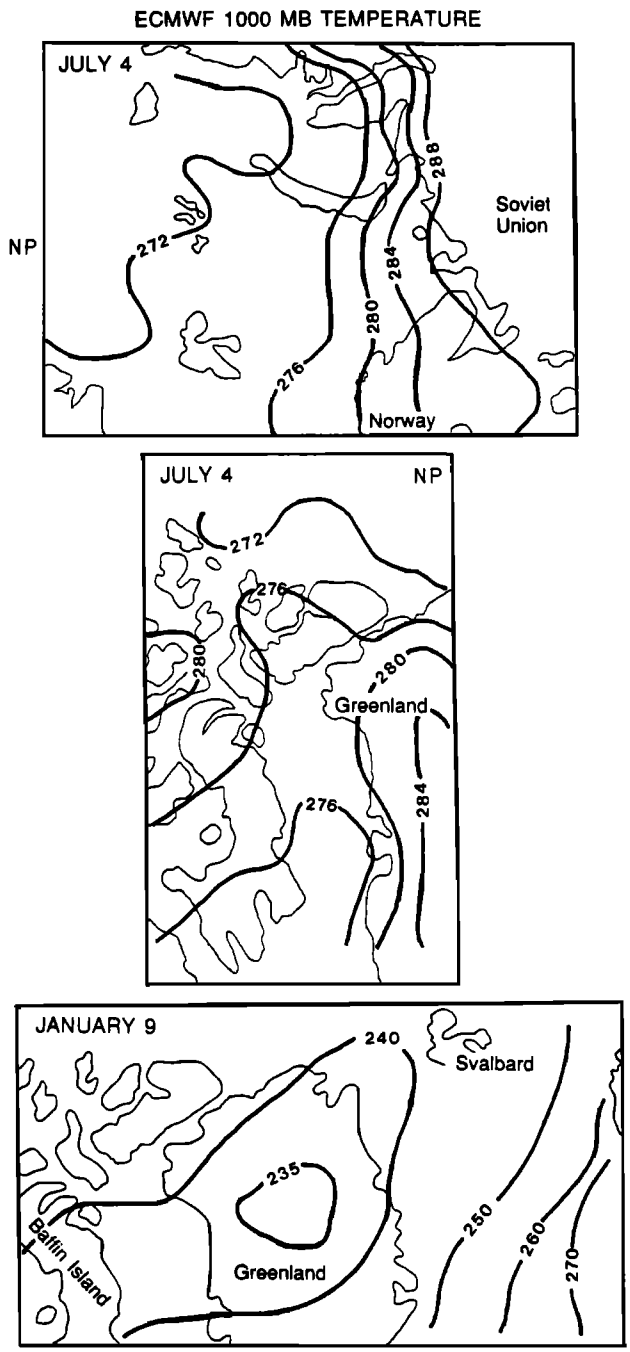

Fig. 8. Surface temperatures in Kelvins from the European Centre for Medium Range Forecasting (ECMWF); July 4, 1984, and January 9, 1984.

to changes in thresholds. Error will propagate from this point, so it is important that all pixels labeled clear in this step actually are clear, but it is also important to obtain as many clear pixels as possible. The spatial test is inappropriate for winter data in polar regions where strong surface temperature inversions are the norm, and is of questionable utility even in the summer when isothermal and inversion conditions are also common. The inclusion of AVHRR channel 3 aids in the discrimination of ice/snow and cloud, and the channel 3-4 difference detects optically thin cloud and fog.

Snow and ice information provided by the SMMR and SMMR-derived data sets was another important addition to the basic algorithm. No other use of SMMR data in conjunction with AVHRR data for polar cloud and surface analysis has been reported in the literature. The merged data sets capitalize on the unique capabilities of AVHRR and passive microwave data by reducing the inherent limitations of each sensor, and provide a means to improve automated cloud mapping in polar regions. Similar analyses will become possible with the suite of remote sensing data due to be collected from the Earth Observing System (EOS) in the 1990s.

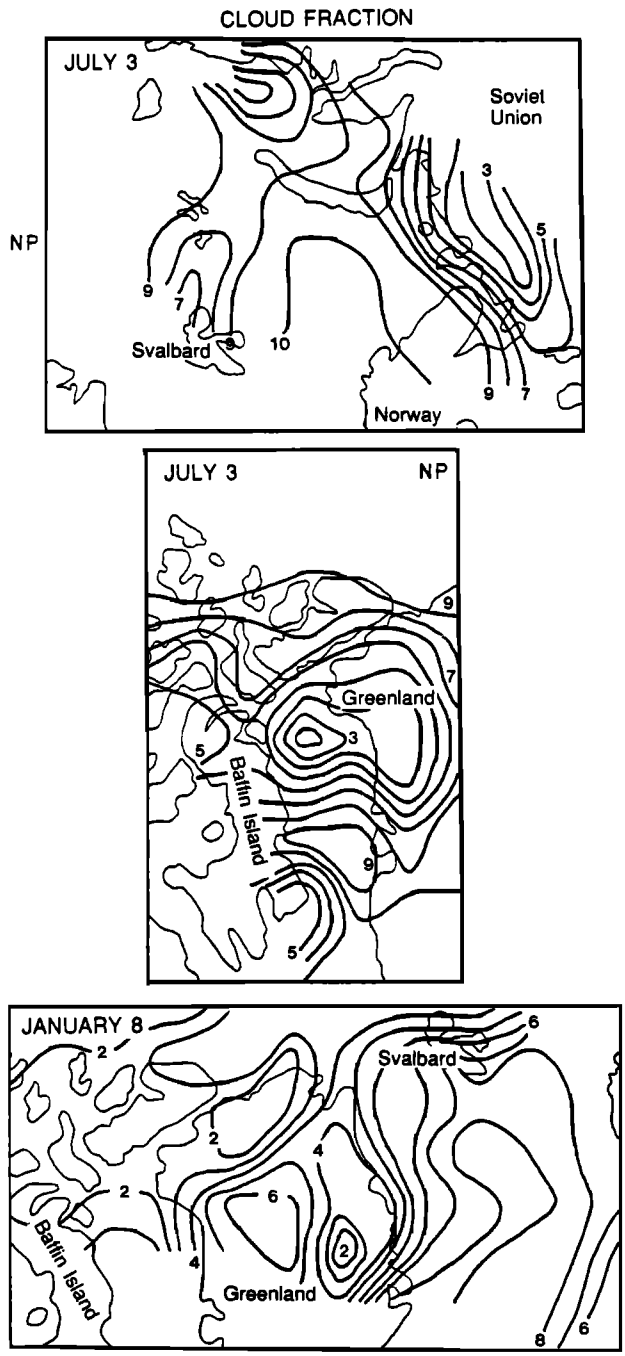

Fig. 9. Cloud fraction for each study area on July 3, 1984, and January 8, 1984, in tenths.

Unfortunately, extracting, calibrating, and registering three or more AVHRR channels for seven days, two SMMR channels for each of 3 days, calculating sea ice concentration for 3 days, and developing a land/ice cap mask is not a trivial undertaking, so that this procedure is cost-effective only in areas where the more basic methods fail; e.g., over snow and ice.

The cloud detection algorithm presented here used as its starting point ideas that were presented in *Rossow et al.* [1985] as design criteria for an emerging ISCCP algorithm. From that point, this algorithm and that of the ISCCP developed for the most part independently. The ISCCP algorithm is currently being applied operationally on a global scale, and data for selected time periods are available for distribution. It is of interest to point out a few similarities and differences between the two algorithms. The basic steps of space/time tests, clear-sky radiance composites, and bispectral thresholds have been retained in current ISCCP algorithms, although some threshold and test values have changed. These are also used here, with these exceptions: the spatial tests are eliminated (section 6.2), the temporal tests are skipped if the pixel is first determined to be thin cloud, and winter thresholds and surface/cloud temperature relationships are treated separately. The importance of surface identification has resulted in the use of SMMR data here (25 km resolution), and the use of NOAA snow cover, U.S. Navy/NOAA sea ice data sets (1° latitude-longitude grid) and land topography data in the ISCCP procedure. Statistical tests for the determination of cloud contamination here are based on probabilities of sample statistics coming from a population defined by previous analyses. In the ISCCP algorithm, average and extremum from radiance distributions are compared over short-term and long-term time periods. The difference between these methods is difficult to assess because the initial classifications would produce different radiance distributions. There are other differences between the two algorithms; *Rossow et al.* [1988] provides greater detail on the ISCCP algorithm. However, the use of correlative data for surface identification and the use of temporal tests have been deemed crucial to both, and should be considered important components of a cloud detection algorithm.

10. CONCLUSIONS

A cloud detection algorithm for use with Arctic AVHRR and SMMR data has been presented. Some of the design objectives for the International Satellite Cloud Climatology Project (ISCCP) cloud detection procedure such as space and time contrasts comprise basic thermal-only and visible/thermal algorithm versions, which are then modified for polar applications. All versions of the algorithm perform best over snow-free land and open water, so that improvement in computed cloud fraction using the modified algorithm will be greater over snow, ice cap, and sea ice and less over open water and snow-free land. In test cases, cloud fraction computed with the modified algorithm was found to be at least 5% more accurate when compared to manual interpretations.

For the data sets employed, the best method of cloud detection with Arctic AVHRR data includes first an accurate identification of surface types and changes. This allows thresholds to be set appropriately, and here is accomplished with SMMR passive microwave data. Next the temporal variability of pixel radiances is examined, using channels 1, 4, and the reflected component of channel 3 during summer and the difference between channels 3 and 4 in conjunction with channels 4 or 5 for winter analyses. Differences between thermal channels aid in the detection of thin cloud. Compositing over a 5-day period provides the clear-sky information for the final multispectral thresholding of the daily data. The lack of "ground truth" makes testing and validation difficult, a problem which can be alleviated to some extent with the use of synthetic data sets.

Acknowledgments. This work was supported under NASA grant NAG-5-898 and a DOD University Research Instrumentation Program grant N00014-85-C-0039. Thanks are due to W. Rossow and E. Raschke for providing AVHRR GAC data. We further thank the reviewers for their suggestions and W. Rossow for his ideas on algorithm design and for valuable comments on an earlier version of this paper.

REFERENCES

Arking, A., and J. D. Childs, Retrieval of cloud cover parameters from multispectral satellite measurements, *J. Clim. Appl. Meteorol.*, *24*, 322-333, 1985.

Barry, R. G., A. Henderson-Sellers, and K. P. Shine, Climate sensitivity and the marginal cryosphere, in Climate Processes and Climate Sensitivity, edited by J. Hansen and T. Takahashi, pp.221-337, *Geophys. Monogr.*, vol.29, AGU, Washington, D.C., 1984.

Barry, R. G., R. G. Crane, A. Schweiger, and J. Newell, Arctic cloudiness in spring from satellite imagery, *J. Climatol.*, *7*, 423-451, 1987.

Bolle, H. J., Assessment of thin cirrus and low cloud over snow by means of the maximum likelihood method. *Adv. Space Res.*, *5*(6), 169-175, 1985.

Brown, O., J. Brown, and R. Evans, Calibration of advanced very high resolution radiometer infrared observations, *J. Geophys. Res.*, *90*(C6), 11,667-11,677, 1985.

Budyko, M. I., The effect of solar radiation variations on the climate of the Earth, *Tellus*, *21*, 611-619, 1969.

Bunting, J. T., and R. F. Fournier, Tests of spectral cloud classification using DMSP fine mode satellite data, *AFGL-TR-80-0181*, Environ. Res. Pap. *704*, 42 pp., Air Force Geophys. Lab., Hanscom Air Force Base, Mass., 1980.

Cavalieri, D. J., P. Gloersen, and W. J. Campbell, Determination of sea ice parameters with Nimbus 7 SMMR, *J. Geophys. Res.*, *89*, 5355-5369, 1984.

Coakley, J. A., Jr., Properties of multilayered cloud systems from satellite imagery, *J. Geophys. Res.*, *88*, 818-828, 1983.

Coakley, J. A., Jr., A dynamic threshold method for obtaining cloud cover from satellite imagery data, *J. Geophys. Res.*, *92*(D4), 3985-3990, 1987.

Coakley, J. A., Jr. and D. G. Baldwin, Towards the objective analysis of clouds from satellite imagery data, *J. Clim. Appl. Meteorol.*, *23*, 1065-1099, 1984.

Coakley, J. A., and F. P. Bretherton, Cloud cover from high-resolution scanner data: Detecting and allowing for partially filled fields of view, *J. Geophys. Res.*, *87*(C7), 4917-4932, 1982.

Colony, R., and E. A. Munoz, Arctic Ocean buoy program, data report, 1 January 1984 - 31 December 1985, 227 pp., Polar Sci. Cent., Univ. of Washington, 1986.

Crane, R. G., and M. R. Anderson, Satellite discrimination of snow/cloud surfaces. *Int. J. Remote Sens.*, *5*, 213-223, 1984.

d'Entremont, R. P., Low- and mid-level cloud analysis using nighttime multispectral imagery, *J. Clim. Appl. Meteorol.*, *25*, 1853-1869, 1986.

d'Entremont, R. P., and L. W. Thomason, Interpreting meteorological satellite images using a color-composite technique. *Bull. Am. Meteorol. Soc.*, *68*(7), 762-768, 1987.

Desbois, M., and G. Seze, Use of space and time sampling to produce representative satellite cloud classifications, *Ann. Geophys.*, *2*(5), 599-606, 1984.

Desbois, M., G. Seze, and G. Szejwach, Automatic classification of clouds on METEOSAT imagery: application to high level clouds, *J. Appl. Meteorol.*, *21*, 401-412, 1982.

Dozier, J., and S. G. Warren, Effect of viewing angle on the infrared brightness temperature of snow, *Water Resour. Res.*, *18*(5), 1424-1434, 1982.

Ebert, E., A pattern recognition technique for distinguishing surface and cloud types in the polar regions, *J. Clim. Appl. Meteorol.*, *26*, 1412-1427, 1987.

Ebert, E., Analysis of polar clouds from satellite imagery using pattern recognition and a statistical cloud analysis scheme, *J. Appl. Meteorol.*, *26*, 1412-1427, 1989.

Garand, L., Automated recognition of oceanic cloud patterns, I, Methodology and application to cloud climatology, *J. Clim.*, *1*, 20-39, 1988.

Gerstl, S. A. W., and C. Simmer, Radiation physics and modelling for off-nadir satellite sensing of non-Lambertian surfaces, Rep. LA-UR-85-4204, Los Alamos Natl. Lab., Los Alamos, N.M., 1985.

Gloersen, P., and D. J. Cavalieri, Reduction of weather effects in the calculation of sea ice concentration from microwave radiances, *J. Geophys. Res.*, *91*(C3), 3913-3919, 1986.

Gorshkov, S. G. (ed.), World Ocean Atlas, vol. 3, Arctic Ocean, Pergamon, New York, 1983.

Harris, R., and E. C. Barrett, Toward an objective neph-analysis, *J. Appl. Meteorol.*, *17*, 1258-1266, 1978.

Hunt, G. E., Radiative properties of terrestrial clouds at visible and infra-red thermal window wavelengths, *Q. J. R. Meteorol. Soc.*, *99*, 346-359, 1972.

Inoue, T., A cloud type classification with NOAA 7 split-window measurements, *J. Geophys. Res.*, *92*(D4), 3991-4000, 1987*a*.

Inoue, T., The clouds and NOAA-7 AVHRR split window, Report of the ISCCP Workshop on Cloud Algorithms in the Polar Regions, Tokyo, Japan, 19-21 August 1986, Rep. WCP-131, WMO/TD-170, Geneva, 1987*b*.

Key, J. R., J. A. Maslanik, and R. G. Barry, Cloud classification using a fuzzy sets algorithm: A polar example, *Int. J. Remote Sens.*, in press, 1989*a*.

Key, J., J. A. Maslanik, and A. J. Schweiger, Classification of merged AVHRR and SMMR data with neural networks, *Photogram. Eng. Remote Sen.*, *55*(9), 1331-1338, 1989*b*.

Lauritson, L., G. G. Nelson, and R. W. Port, Data extraction and calibration of TIROS-N/NOAA A-G radiometer, *NOAA Tech. Memo.*, NESS 107, 81pp., 1979.

Maslanik, J. A., J. R. Key, and R. G. Barry, Merging AVHRR and SMMR data for remote sensing of ice and cloud in the polar region. *Int. J. Rem. Sens.*, in press, 1989.

McGuffie, K., and D. A. Robinson, Examination of USAF Nephanalysis performance in the marginal cryosphere region. *J. Clim.*, *1*(11), 1124-1137, 1988.

Minnis, P., E. F. Harrison, and G. G. Gibson, Cloud cover over the equatorial eastern Pacific derived from July 1983 International Satellite Cloud Climatology Project data using a hybrid bispectral threshold method, *J. Geophys. Res.*, *92*(D4), 4051-4073, 1987.

Minnis, P., and E. F. Harrison, Diurnal variability of regional cloud and clear sky radiative parameters derived from GOES data, I. Analysis method, *J. Clim. Appl. Meteorol.*, *23*, 993-1011, 1984.

NOAA, *NOAA Polar Orbiter Data User's Guide*, U.S. Dep. of Commer., Natl. Ocean. and Atmos. Admin., NESDIS, February 1984.

Olesen, F., and H. Grassl, Cloud detection and classification over oceans at night with NOAA-7, *Int. J. Remote Sens.*, *6*(8), 1435-1444, 1985.

Pairman, D., and J. Kittler, Clustering algorithms for use with images of clouds, *Int. J. Remote Sens.*, 7(7), 855-866, 1986.

Parikh, J. A., A comparative study of cloud classification techniques, *Remote Sens. Environ.*, *6*, 67-81, 1977.

Polar Research Board, *The Polar Regions and Climatic Change*, 59pp., National Research Council, National Academy Press, Washington, D. C., 1984.

Raschke, E., Cloud analysis of AVHRR data measured over polar regions, Report of the ISCCP Workshop on Cloud Algorithms in the Polar Regons, Rep. WCP-131, WMO/TD 170, Tokyo, Japan, 19-21 August 1986, Geneva, 1987.

Robock, A., and D. Kaiser, Satellite-observed reflectance of snow and clouds, *Mon. Weather Rev.*, *113*(11), 2023-2029, 1985.

Rossow, W. B., Measuring cloud properties from space: A review, *J. Clim.*, *2*, 201-213, 1989.

Rossow, W. B., F. Mosher, E. Kinsella, A. Arking, M. Desbois, E. Harrison, P. Minnis, E. Ruprecht, G. Seze, C. Simmer, and E. Smith, ISCCP cloud algorithm intercomparison, *J. Clim. Appl. Meteorol.*, *24*, 877-903, 1985.

Rossow, W. B., L. C. Garder, P.-J. Lu, and A. Walker, The International Satellite Cloud Climatology Project documentation of cloud data, *Rep. WMO TD266*, World Meteorol. Org., December 1988.

Rossow, W. B., C. L. Brest, and L. C. Garder, Global, seasonal surface variations from satellite radiance measurements, *J. Clim.*, *2*, 214-247, 1989*a*.

Rossow, W. B., L. C. Garder, and A. A. Lacis, Global, seasonal cloud variations from satellite radiance measurements, I. Sensitivity of analysis, *J. Clim.*, *2*, 419-458, 1989*b*.

Saltzman, B., and R. E. Moritz, A time-dependent climatic feedback system involving sea-ice extent, ocean temperature, and CO_2, *Tellus*, *32*, 93-118, 1980.

Saunders, R. W., An automated scheme for the removal of cloud contamination from AVHRR radiances over western Europe. *Int. J. Remote Sens.*, *7*(7), 867-886, 1986.

Saunders, R. W., and K. T. Kriebel, An improved method for detecting clear sky and cloudy radiances from AVHRR data, *Int. J. Remote Sens.*, *9*, 123-150, 1987.

Scharfen, G., R. G. Barry, D. A. Robinson, G. Kukla, and M. C. Serreze, Large-scale patterns of snow melt on arctic sea ice mapped from meteorological satellite imagery, *Ann. Glaciol.*, *9*, 1-6, 1987.

Serreze, M. S., and R. G. Barry, Synoptic activity in the Arctic Basin, 1979-85, *J. Clim.*, *1*, 1276-1295, 1988.

Shenk, W. E., and R. J. Curran, A multi-spectral method of estimating cirrus cloud top heights, *J. Appl. Meteorol.*, *12*, 1213, 1973.

Shenk, W. E., R. J. Holub, and R. A. Neff, A multispectral cloud type identification method developed for tropical ocean areas with Nimbus-3 MIRR measurements, *Mon. Weather Rev.*, *104*, 284, 1976.

Shine, K. P., and R. G. Crane, The sensitivity of a one dimensional thermodynamic sea ice model to changes of cloudiness, *J. Geophys. Res.*, *89*(C6), 10,615-10,622, 1984.

Steffen, K., Bidirectional reflectance of snow at 500-600 nm, Large Scale Effects of Seasonal Snow Cover (Proceedings of the Vancover Symposium, August 1987). IAHS Publ., 166, 415-425, 1987.

Susskind, J., D. Reuter, and M. T. Chahine, Cloud fields retrieved from analysis of HIRS2/MSU sounding data, *J. Geophys. Res.*, *92*(D4), 4035-4050, 1987.

Welch, R. M., S. K. Sengupta, and D. W. Chen, Cloud field classification based upon high spatial resolution textural features, 1, Gray level co-occurrence matrix approach, *J. Geophys. Res.*, *93*(D10), 12,663-12,681, 1988.

Wiscombe, W. J. and S. G. Warren, A model for the spectral albedo of snow. I: Pure snow, *J. Atmos. Sci.*, *37*, 2712-2733, 1980.

World Meteorological Organization (WMO), Report of the ISCCP workshop on cloud algorithms in the polar regions, Tokyo, Japan, 19-21 August 1986, World Clim. Res. Prog., *Rep. WCP-131, WMO/TD 170*, 19-21 August 1986, Geneva, 1987.

World Meteorological Organization (WMO), Report of the third session of the working group on sea ice and climate, *Rep. WCRP-18, WMO/TD 272*, Oslo, Norway, May 13 to June 3, 1988.

R. G. Barry, and J. Key Cooperative Institute for Research in Environmental Sciences, University of Colorado, Campus Box 449, Boulder, CO 80309.

(Received March 1, 1989;
revised June 29, 1989;
accepted July 6, 1989.)